How long do geomagnetic reversals take?

Moritz Heimpel (mheimpel@ualberta.ca)
University of Alberta https://orcid.org/0000-0003-2965-8271
Michael Evans
University of Alberta

Physical Sciences - Article

Keywords: Geomagnetic, polarity, reversals, Earth, core, Dynamo models

Posted Date: May 29th, 2023

DOI: https://doi.org/10.21203/rs.3.rs-2860867/v1

Additional Declarations: There is **NO** Competing Interest.

How long do geomagnetic reversals take?

Moritz H. Heimpel[1*] and Michael E. Evans[1†]

[1*]Department of Physics, University of Alberta, Edmonton, Alberta, Canada.

*Corresponding author(s). E-mail(s): mheimpel@ualberta.ca;
†These authors contributed equally to this work.

Abstract

The duration of magnetic field reversals at locations on Earth is variable, with estimates ranging from less than one hundred years [1–3] to thousands of years [4–7]. Simple physical models of the reversal process predict short reversal duration near the poles, and longer duration near the equator [8, 9]. However, a compilation of palaeomagnetic observations finds the opposite [4]. Here we resolve this long-standing paradox using palaeomagnetic data and an Earthlike [10], reversing dynamo simulation. We identify two types of local reversals for a global magnetic reversal in our simulation. Simple local reversals (SLR) undergo a single polarity flip, with durations of 109 years – 2.32 kyr. Complex local reversals (CLR) flip more than once, with durations of 1.40 kyr – 13.2 kyr. While SLR occurrence and duration peaks near the equator and diminishes at mid-latitudes, CLR occurrence and duration peaks near the poles. Surprisingly, equatorial latitudes are free of CLR and polar regions are free of SLR. These results are consistent with the simple physical models and palaeomagnetic observations. We find that analysis of the local and global magnetic field behaviour in our dynamo model can reconcile the complex and seemingly contradictory picture of magnetic reversals that has emerged from the analysis of high-quality volcanic and sedimentary records.

Keywords: Geomagnetic polarity reversals Earth core Dynamo models

1 Introduction

1.1 Palaeomagnetic Reversal Durations

The fact that the geomagnetic field switches polarity from time to time is no longer in doubt. But questions remain as to the process involved, and how long it takes. Early palaeomagnetic observations on Icelandic lava flows provided estimates for polarity transitions of 5 kyr [11] and 1-3 kyr [12], although Einarsson [13] suggested that "even a few centuries might in most cases be sufficient". Such estimates are limited by the highly variable rate of volcanic activity, so other workers eventually turned to sedimentary records.

Of particular promise are sediments in the deep ocean where depositional rates are likely to be fairly constant. Opdyke et al. [14] derived a value of about 4600 years from sediments in the southern Indian Ocean. More recently, Clement [4] has summarized the sedimentary record (mostly marine, but including a few cases from continental sites) and arrived at an overall mean duration of 7± 1 kyr. Subsequently, five high-resolution North Atlantic cores yielded reversal durations between 2.9 and 6.2 kyr, with a mean of 4.4 ± 1.3 kyr [15]. Leonhardt and Fabian [16] developed an inversion model using both directional and palaeointensity data, from which they obtained a global picture of the evolution of the geomagnetic field during the Brunhes-Matuyama (BM) transition. They find durations between 1 and 10 kyr, depending on site location. Overall, they obtain a global average of 5200 years – essentially what Hospers said at the outset. Having come full circle, it would seem that the matter is closed. But there is evidence that reversals can sometimes be much faster, durations on the order of a decade having been claimed.

Okada and Niitsuma [1] report palaeomagnetic results from a siltstone sequence outcropping on the Boso Peninsula, Japan. They make the remarkable claim that the BM transition lasted only 38 years. Closer inspection reveals that the position of the Virtual Geomagnetic Pole (VGP) is erratic in the stratigraphic interval involved, crossing the equator five times. Fluctuations like these are sometimes due to differential remanence lock-in, as seen in the Chinese loess [17]. But they can also arise from the natural behaviour of the relatively enhanced non-dipole field during reversals.

Two geological sections in Italy have recently provided evidence of a rapid BM transition, one located near Sulmona in central Italy, the other 450 km to the Southeast, near Crotone [3]. At Sulmona, the BM transition was originally regarded as lasting

"less than 13+/-6 years" [18], but further work demonstrated that the sediments are prone to remagnetization [19, 20].

Brown et al. [21] take an entirely different approach to reversal duration, based on the secular variation derived from the CALS7K.2 model [22], which is a global summary of archaeomagnetic and palaeomagnetic observations spanning the last 7000 years (16,085 declination values, 13,080 inclination values, and 3188 intensity values). To mimic reversal behaviour, they superimpose a dipole that changes monotonically from +g10 to -g10 over the entire 7000 years. Defining the duration of a directional reversal as the time interval that the VGP spends between 45°N and 45°S leads to reversals spanning a wide range, from less than 10 years to more than 1000 years, depending on geographic location. Brown and co-authors show two examples of "fast" reversals, but only one of them (Tahiti) can be regarded as "sub-decadal". The other (Mexico) exhibits a more complicated evolution spanning several centuries (see their Fig. 4b). As pointed out above, complications of this kind simply reflect non-dipole behaviour during reversals. They are seen in many of the examples shown by Brown and co-authors, as well as in real palaeomagnetic sequences (see above), and in geodynamo simulations (see below). Their effect is to increase the duration of directional reversals. Very rapid reversals may occur at some locations, but the global map derived by Brown et al. [21] indicates that $> 90\%$ of sites have reversal durations exceeding 200 years, with many cases exceeding 1500 years.

1.2 Previous reversing dynamo modelling results

Building on early self-consistent spherical dynamo models [23], subsequent dynamo models included different heat-flow patterns at the core/mantle boundary (CMB). Two patterns are particularly important: homogeneous (spatially uniform heat flux boundary conditions) and tomographic (heat flux patterned after seismic velocity of the lowermost mantle) [24, 25]. Glatzmaier et al. [24] reported two homogeneous cases yielding reversals lasting $\sim$ 1000 years, and two tomographic cases with reversals of longer durations, 6 kyr and $>$ 20 kyr. Considerable complexities of specific reversals were presented for the later models [25], including one of 22 kyr duration, in which the middle 3 kyr contained seven polarity changes. Other reversals were simpler and faster (2-7 kyr), but also exhibited rapid fluctuations, sometimes caused by patches of vertical magnetic flux that intensified in a matter of centuries [25].

Olson et al. [26] compared the complexity of reversals and excursions in dynamo models to palaeomagnetic observations. For a global reversal, they describe the reversal

process as being composed of three distinct stages: relatively long timescale intensity reduction, multipolarity, which can include precursory reversal and recovery to the original polarity, and final directional polarity reversal. This last directional polarity reversal stage can be rapid: "the dipole latitude changes by 130° in about 400 years" [26].

The dynamo models of Wicht [27] yielded reversal durations that depended on site location, with longer durations at the poles than at the equator, which is consistent with our results. The resulting range of reversal durations, 3.3 kyr to 34.8 kyr [27], is comparable with the longer durations found in our simulation. In a later study Wicht et al. [28] obtained durations of order 10 kyr. However, it is difficult to compare those studies to ours, since they did not distinguish between simple and complex reversals. Also, the high Ekman numbers in those studies ($E \geq 10^{-3}$) [27, 28] likely precluded the occurrence of a population of shorter duration local reversals found in our simulation.

2 Results

2.1 Reinterpretation of fast palaeomagnetic reversals

Figure 1 shows the Brunhes-Matuyama reversal from three sites, the Yanagawa section, Japan, the Valle di Manche (VdM) section near Crotone, Italy, and ODP hole 1063A, Bermuda Rise [15]. Okada and Niitsuma [1] obtained their transition duration estimate of 38 years from what they called "the last swing of the VGP in the Brunhes-Matuyama boundary", which they claimed spans 14 cm. However, we argue here that the entire polarity transition occupies a much thicker zone of about 67 cm (Fig. 1a,b). Also, using modern values for the ages of the Brunhes-Matuyama boundary and Marine Isotope Stage 19, we update the sedimentation rate to 270 cm/kyr (instead of the old values used by Okada and Niitsuma, which implied 370 cm/kyr). Thus we obtain a reversal duration of ~ 250 years.

The suggestion that the BM transition may have lasted only 13±6 years has been superseded: Sagnotti et al. [19] now suggest that the time taken by the transition was "perhaps in the range of 100 yr". Macrì et al. [3] arrive at essentially the same conclusion for the VdM section. At both localities, the polarity switch occurs between adjacent samples, with no intermediate remanence directions observed. However, the VdM section has a normal-polarity zone about 15-30 cm below what Macri and co-authors call "the end of the M-B transition". The magnetic behaviour exhibited by some of the samples in this zone leads the authors to suggest that "this interval

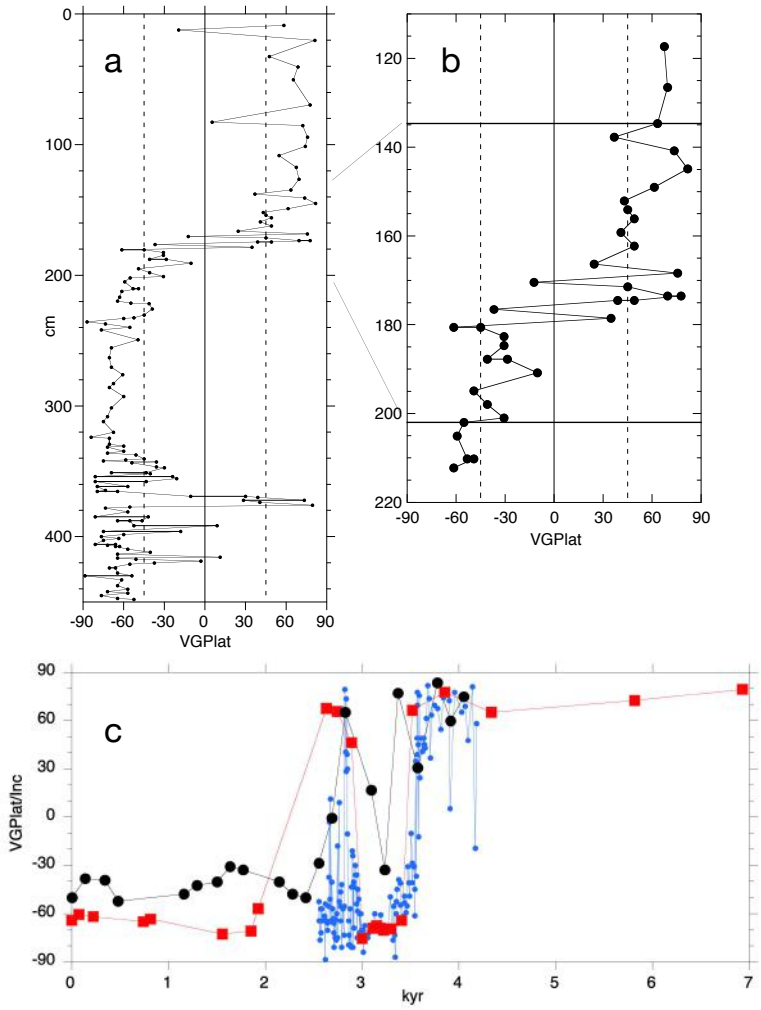

Fig. 1 Brunhes-Matuyama reversal from a & b) the Yanagawa section, Japan, adapted from Figure 7 of Okada and Niitsuma [1]. b) The enlarged plot shows details of the polarity transition, which spans 67 cm (indicated by the horizontal lines). c) VGP latitude is plotted for the Valle di Manche (VdM) section, Italy (red) the Yanagawa section, Japan (blue), ODP hole 1063A, Bermuda Rise discrete-sample inclinations (black). Time is plotted horizontally to facilitate comparison with the dynamo simulation discussed below. The zero for each time series is chosen to achieve a good visual fit.

probably reflects remagnetization" [3]. But other samples give high-quality results. We suggest that these are reliable recorders of typical geomagnetic instability, including low-latitude VGPs, within a longer polarity transition lasting 1000 years or more (Fig. 1c). This interpretation is strongly supported by the corresponding results from the

Yanagawa section, where normal polarities also occur a couple of metres prior to the final polarity switch (compare Fig. 1a and 1c).

2.2 Dynamo model results

2.2.1 Zonal Gauss coefficients and Reversal Angle

Time series spanning the magnetic reversal from our dynamo simulation are shown in Fig. 2. The top panel shows the first three zonal Gauss coefficients: $g_{1,0}$ (dipole), $g_{2,0}$ (quadrupole) and $g_{3,0}$ (octupole) over several dipole decay times τ_d. The middle panel shows the global mean of the local reversal angle $\langle \alpha_r \rangle_{\theta,\phi}$, where the mean is over θ, ϕ (see Methods, eq. 1). This global mean is seen to be a simple reversal (see definition in Methods), with duration $0.018\tau_d = 1008$ years. Also shown for Fig. 2, over a shorter time scale centred on the dipole reversal, are images of the ϕ–averaged reversal angle $\langle \alpha_r \rangle_\phi$, and α_r at a certain longitude ϕ. The images of reversal angle show that local reversals are quite rapid; the reversal time scale at a particular latitude, or location is typically ~ 1 kyr – much shorter than the time scale required for the dipole to reverse between saturated polarities (~ 100 kyr or ~ 2 dipole decay times). Multiple local excursions and double reversals occur over the timespan of the single global reversal. These local excursions and reversals are seen to be more prevalent at high latitudes.

Black arrows for the images of Fig. 2 indicate the time for what we identify as the reversal event near each pole. The model shows significant upper (north) – lower (south) hemispheric asymmetry in the timing of the polar reversal event, with a difference between north and south reversal times of $\simeq 800$ years, which is comparable to the global mean reversal duration of 1008 years. We note that grid points are not placed at the poles of our model. Rather, the proximity to the pole of the highest latitude grid point depends on the grid resolution. Still, given the spherical geometry, near the poles the longitudinally averaged reversal angle time series is nearly equivalent to that for a given longitude.

The images in Fig. 2 show that the local character of the full transition from one magnetic polarity to the reverse is different at the poles than at the equator. Near the poles the transition from one polarity to the other is more strongly punctuated by excursions and double reversals. This polar transitional time period (~ 20 kyr) is much greater than the local reversal time period (~ 1 kyr), and much greater than the north – south main reversal event time difference (also ~ 1 kyr). Excursions and double reversals are less prevalent near the equator. At low latitudes fluctuations in

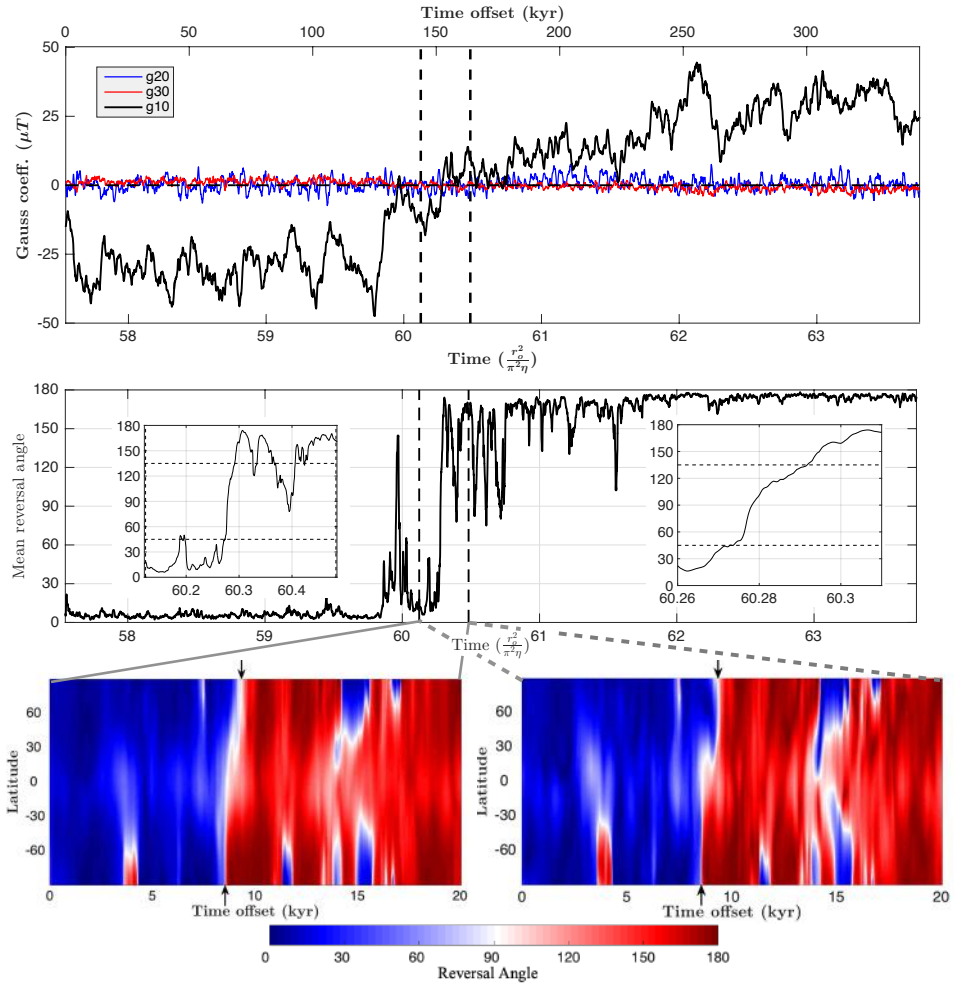

Fig. 2 Top: Dynamo model time series of the first three zonal Gauss coefficients, dipole component (black), quadrupole (blue), and octupole (red). Vertical dashed lines indicate the time interval in which reversal angle displayed in bottom images. Middle: Global mean local reversal angle $\langle \alpha_r \rangle_{\theta,\phi}$. Two inset plots zoom in on the mean directional reversal. Horizontal dashed lines at $\theta = 45°, 135°$ mark the initiation and termination angles that define a reversal (see Methods). Bottom left: longitudinally averaged reversal angle as a function of time and latitude. Bottom right: reversal angle as a function of time and latitude at longitude $\phi = 60°$. The arrows in the bottom two images indicate the reversal times near the poles, and are placed at a time offset of 8.55 kyr (latitude $\simeq -90$, bottom of each image) and 9.35 kyr (latitude $\simeq 90$, top of each image).

the reversal angle are seen to be strongest in the time interval between the north and south main reversal event (time interval between black arrows). In other words,

complex reversals typically occur at high latitudes, whereas simple reversals tend to occur at low latitudes Furthermore simple reversals tend to have longer duration at low latitudes, due to the north – south time offset of local reversals.

2.2.2 Local Reversal Duration

Whereas the timing of global and local reversals is shown in Fig. 2, we focus on local reversal duration in Fig. 3. The top image shows a map of the local reversal duration as a function of location. The two types of reversals, simple and complex are shown with two colour palettes on the map. Below the map four plots detail the reversal angle over time at locations marked on the map. To show the range of local reversal behaviours, we display examples of relatively short and relatively long reversals of both types (simple and complex).

Simple reversals tend to occur at low latitudes, mostly within 30° of the equator, whereas complex reversals tend to occur at higher latitudes and near both poles. Since complex reversals typically have longer duration than simple reversals polar, higher latitudes tend to have longer reversal durations. Equatorial reversal durations are of order 1 kyr, whereas high latitude durations are of order 10 kyr. The two simple reversals shown in Fig. 3 are at -30° and 0° latitude and have durations 0.21 kyr and 1.94 kyr respectively. The two complex reversals are at 30° and -60° latitude and have durations 7 kyr and 12.37 kyr respectively.

2.2.3 Latitudinal dependence of reversal duration

Longitudinally averaged reversal durations are plotted as a function of latitude in Fig. 4. The set of all reversal durations (including SLR and CLR) shows durations are greater at the poles by a factor of about 10 compared to those near the equator. However, the latitudinal distribution of reversal durations becomes more interesting when considering SLR and CLR reversal populations separately. Simple local reversals, which occur at mid to equatorial latitudes, have about 5× longer durations at the equator than at mid-latitudes. In contrast, CLR, which do not occur near the equator, have roughly 2× longer durations at the poles than at mid-latitudes (see also Supplementary Information, Fig. A1).

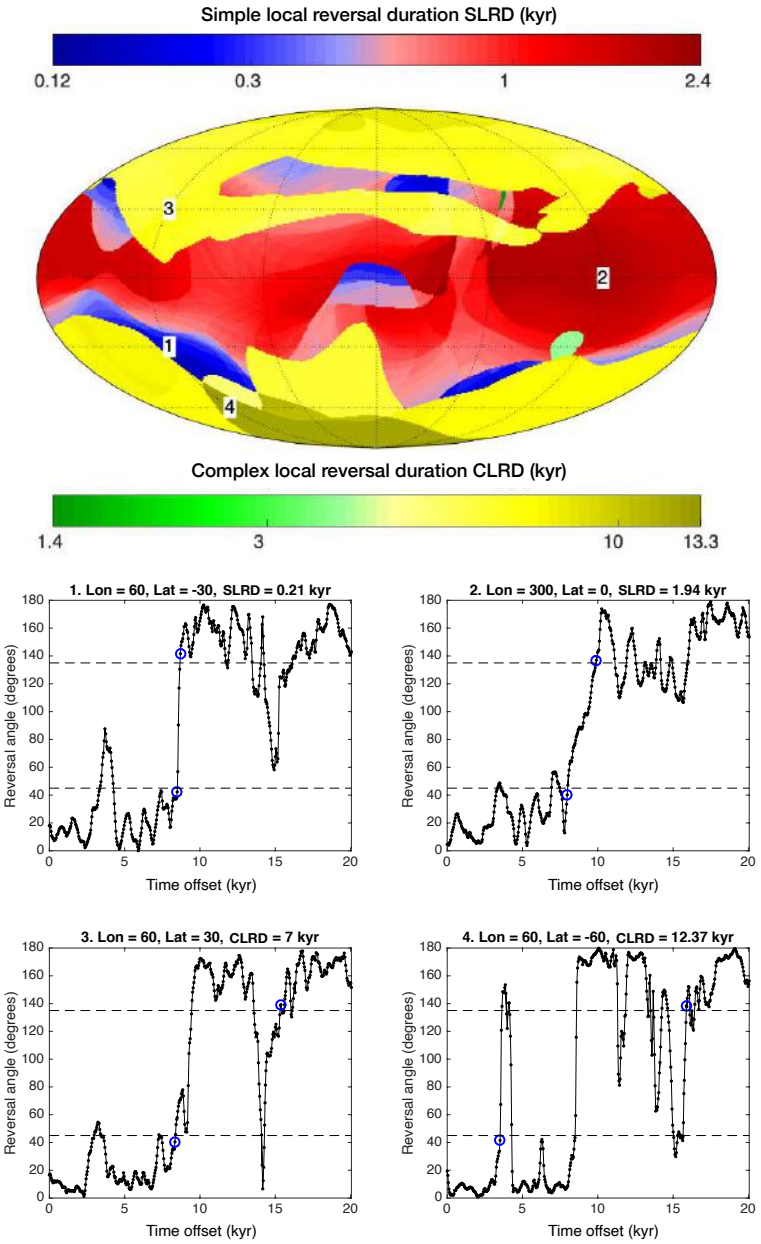

Fig. 3 Dynamo model reversal duration. Simple and complex local reversal durations (SLRD and CLRD) are shown with two colour scales. Numbers on Mollwied projection indicate the locations of labelled example time series below. Blue circles on the time series show the beginning and ending data points defining the reversal durations.

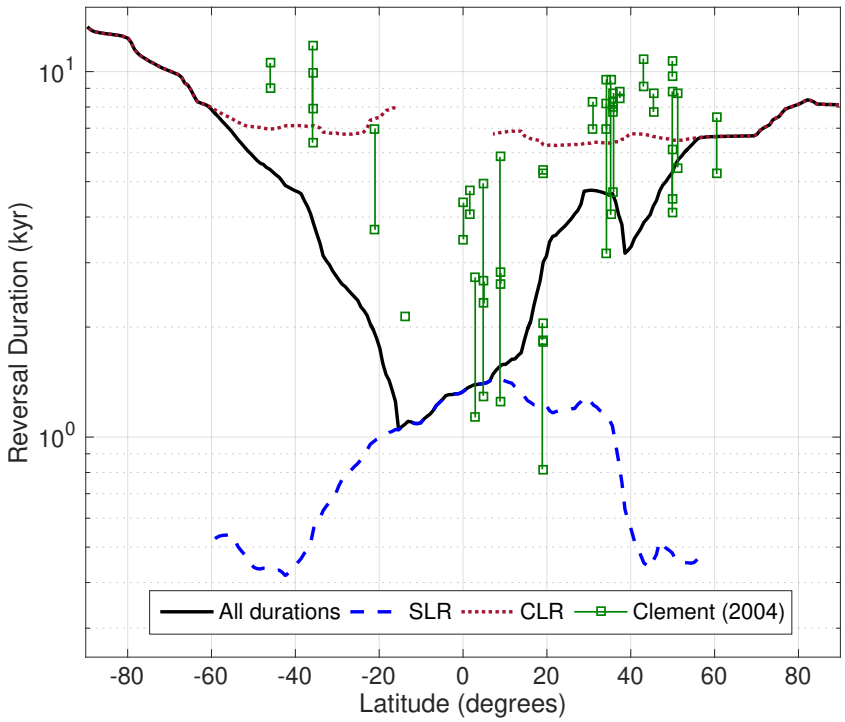

Fig. 4 Longitudinally averaged reversal duration as a function of latitude for all local reversal durations (black solid line), and for simple (dashed blue line) and complex local reversal durations (dotted red lines). Dark green lines show Brunhes-Matuyama, Upper and Lower Jaramillo, and Upper Olduvai data from Table 1 and Figure 2 of [4], with bounding markers representing lower and upper duration.

3 Discussion

As was pointed out many years ago, a vector field that reverses by decreasing in magnitude and then building up in the opposite direction "would give a discontinuous change in dip as the field passed through zero however slowly the field decayed" [29]. At all locations, a sudden 180° jump in inclination and declination would be observed. The inclusion of higher-order terms modifies the outcome. For example, a fixed 10% quadrupole component results in a reversal duration of $0.2T$ at the equator (where the reversal duration is defined as the time required for the reversal angle to transit from 45° to 135°, and T is the total time for the dipole to decay (linearly) from +1 to −1). If $T = 7$ kyr [21], the reversal will take 1400 years. At the poles, however, a

discontinuous jump still occurs. Between the poles and the equator, reversals of a few centuries will be observed, as suggested by Einarsson [13].

The simple pattern discussed above, with short duration reversals at the poles and longer duration reversals at the equator, was predicted by heuristic models [8, 9]. In contrast, a global summary of palaeomagnetic reversals based on sedimentary records found the opposite of what was predicted: reversal durations shorter ($\sim$ 1 kyr) near the equator and maximum ($\sim$ 10 kyr) at the highest recorded latitudes [4]. This pattern, with minimum reversal duration near the equator, is reproduced in our simulation when considering all reversals, including SLR and CLR (Fig. 4). However, when SLR and CLR are counted separately it is seen that the SLR follow the opposite pattern, with a maximum in reversal duration at the equator, minimum duration at mid-latitudes and latitudes greater than $\sim 60^\circ$ free of SLR. Thus, our model reproduces both the heuristic models described above and the palaeomagnetic observations.

Although we argue against the very fast (decadal) reversals reported from Japan and Italy [1, 2], our reinterpretations leave them as relatively fast (centennial) features. It is interesting that observations of these fast magnetic reversals were found in sedimentary sequences at mid-latitude: 35° for [1], and $\sim 42^\circ$ for [18] (See Fig. 1). For our simulation the SLR have maximum longitudinally averaged duration near the equator of $\sim$ 1.5 kyr, and decrease steeply in duration, with a band of low durations ($\sim$ 450 years) between 40° and 60° in both hemispheres. Thus our model results are consistent with finding the lowest duration magnetic reversals at mid-latitudes.

4 Methods

We use the numerical dynamo code MAGIC [30–32], to run a high-resolution, Earthlike [10, 33, 34], reversing dynamo simulation (See also Supplementary Information). The code solves the magnetohydrodynamic conservation equations of mass, momentum, energy and magnetic flux for an electrically conducting, Boussinesq or anelastic fluid in spherical geometry. We run MAGIC in Boussinesq mode.

4.1 Parameters and boundary conditions

The non-dimensional governing equations are scaled by four dimensionless parameters: the Prandtl number ν/κ, which is the ratio of viscous and thermal diffusivities; the magnetic Prandtl number $Pm = \nu/\eta$, where η is the magnetic diffusivity; the Ekman number $E = \nu/(\Omega\, D^2)$, where Ω is the rotation rate and $D = r_o - r_i$ is the shell

depth with r_o and r_i, the outer and inner sphere radii; and the Rayleigh number $Ra = \epsilon g D^3/(\kappa\nu)$, where g is gravity and ϵ is a dimensionless volumetric thermal source or sink that balances the integrated thermal flux at the inner and outer boundaries [35]. The velocity boundary conditions are rigid (no slip) at the top (CMB) and bottom (ICB). The inner core, which is modelled as a rigid sphere of the same density and electrical conductivity as the fluid outer core, is free to rotate according to viscous and magnetic torques. The magnetic field outside the core is assumed to be a potential field, meaning the mantle is assumed to be electrically insulating. Thermal boundary conditions are described below.

Table 1 shows parameters, resolution and boundary conditions for the model, and corresponding values for the Earth.

Earth and dynamo model parameters

Parameter	Earth	Model
E	$\sim 10^{-15}$	3×10^{-5}
Ra	$\sim 10^{23}$	2.5×10^{9}
Pr	~ 0.04	1
Pm	$\sim 10^{-6}$	2
$\overline{Rm}$	~ 1800	1174
r_i/r_o	0.35	0.35
n_r		97
l_{max}		160
Run time, τ_d (kyr)		24 (1366)

Table 1 Parameters for Earth's core and the numerical simulation. The radial grid resolution is for the fluid outer core, with n_r the number of radial grid points. An additional 25 radial grid points cover the solid, electrically conductive inner core. The maximum spherical harmonic degree is l_{max}. The number of grid points in ϕ is $n_\phi = 3\,l_{max} = 480$. The number of grid points in θ is $n_\theta = n_\phi/2$. For the outer core radius $r_o = 3485$ km and a liquid iron magnetic diffusivity $\eta = 0.7$ m^2/s, the magnetic timescale $\tau_d = r_o^2/(\pi^2\eta) = 56$ kyr. The model input parameters are E, Ra, Pr and Pm. The model time-averaged Reynolds number $\overline{Rm}$, is an output parameter (result) calculated after the simulation. Earth values from Jones and Schubert [36].

To model thermochemical convection in the Earth's core, we invoke the co-density formulation [35, 37], in which ϵ is a thermal sink that balances the inner boundary

(ICB) buoyancy flux, and the outer boundary (CMB) buoyancy flux is set to zero. Growth of the Earth's solid inner core produces buoyancy by the release of latent heat and light element enrichment at the ICB [37]. Accumulation of light element enriched fluid could result in a stably stratified layer near the CMB [38]. There has been recent interest in seismological observations that support the existence of such a layer [39, 40]. However, other seismically determined models do not require a stably stratified layer [41], and it is not clear that it would survive outer core convective mixing. Recent dynamo modelling that included many cases varying the thickness of a stably stratified layer at the top of the outer core concluded that a stably stratified layer there is not favoured [42]. Still, it is likely that for a large part of Earth's cooling history, including the present era, buoyancy flux is concentrated at the ICB, with small positive or negative buoyancy production at the CMB.

4.2 Magnetic field and time scaling

The numerical model magnetic field strength is scaled in Tesla by $\sqrt{\rho\mu_0\eta\Omega}$, where ρ is the density and μ_0 is the vacuum permeability, η is the magnetic diffusivity, and Ω is the planetary rotation rate. To scale time we use the dipole decay timescale $\tau_d = r_o^2/(\pi^2\eta)$, where r_o is the outer core radius. The scaling of magnetic field strength and time has recently been revised according to new estimates of η. Previous work on numerical dynamos, [43, 44] and core dynamics [36] have used a value of $\eta = 2$ m^2/s. Laboratory experiments of pure Fe have yielded estimates of $\eta = 1$ m^2/s [45, 46], but some recent ab-initio numerical studies have found lower values [47, 48]. However, turbulent advection could lead to a larger effective diffusivity [36]. Here we follow a review of the recent constraints on core properties and dynamics [49], and use an estimated magnetic diffusivity of $\eta = 0.7$ m^2/s, which yields a dipole decay time of $\tau_d = 56$ kyr.

4.3 Reversal angle

The reversal angle as a function of latitude, longitude and time is given by

$$\alpha_r(\theta, \phi, t) = \cos^{-1}\left(\frac{\boldsymbol{B}\cdot\boldsymbol{B}_{ax}}{BB_{ax}}\right), \tag{1}$$

where $\boldsymbol{B}$ & B are the magnetic field vector and its magnitude, respectively, and $\boldsymbol{B}_{ax}$ & B_{ax} are the axial dipole field vector and its magnitude, respectively, before the reversal. Thus, α_r is the angle between the current field vector and the axial dipole

field vector before the reversal. For our simulation $\alpha_r(\theta, \phi, t)$ is calculated at a radius that corresponds to the Earth's surface, which is outside the dynamo region.

4.4 Reversal duration and identification of reversal types

Global reversals generally occur on a longer time scale than local reversals. For our model, during a single global reversal, the local magnetic field, at a particular (θ, ϕ) location and radius corresponding to Earth's surface, may reverse once (simple local reversal) or multiple times (complex local reversal).

A global reversal is identified when the dipole (intensity of the $g_{1,0}$ Gauss coefficient) changes sign. For a given global reversal we seek an algorithm that identifies a local reversal automatically. To achieve this, we choose a time interval that includes a global reversal. A local reversal at a given latitude and longitude occurs when the reversal angle $\alpha_r(\theta, \phi, t)$ goes from an initiation angle of 45° to a termination angle of 135°. Reversal duration is defined by scanning forward and backward in time. We start at the beginning of the chosen time interval, where $\alpha_r < 45°$. The reversal angle is scanned forward in time until the first time-step at which $\alpha_r > 135°$. That time-step is called t_{f2}, where the first subscript (f or b) denotes forward or backward, and the second subscript indicates the termination angle (2 for 135°, 1 for 45°). From t_{f2} we scan backwards in time to t_{f1}, where $\alpha_r < 45°$. We then repeat a similar pair of steps in the other time direction, scanning backward from the end of the chosen time interval to t_{b1}, where $\alpha_r < 45°$, and then forward in time to t_{b2}, where $\alpha_r > 135°$. In all cases the local reversal duration is defined as

$$\mathrm{LRD} = t_{b2} - t_{f1}. \tag{2}$$

Two types of local reversals can result in the duration given by (2). We define a simple local reversal (SLR) to occur where $t_{f2} > t_{b1}$, and a complex local reversal (CLR) otherwise ($t_{b1} \geq t_{f2}$). Note that for SLR $t_{f2} = t_{b2}$ and $t_{b1} = t_{f1}$. CLR are typically but not always of longer duration than SLR.

Appendix A Supplementary material

A.1 Earthlike reversing dynamo

Five snapshots of the radial magnetic field from our simulation are shown in Fig. A1. The first snapshot (a) shows the field at $0.78\tau_d$ before reversal. Here the field is

typical in its dominantly dipolar morphology and high intensity away from a reversal or excursion. The second snapshot (b) shows the field at zero time-offset for the bottom images in Fig. 1. Here, the field is still in the original polarity, with weakened intensity, having undergone an excursion (see Fig. 1, middle panel). The third image (c) shows the field at the time of dipole reversal, with $\alpha_r = 0$. The final two images (d, e) show gradual recovery of the field in reversed polarity.

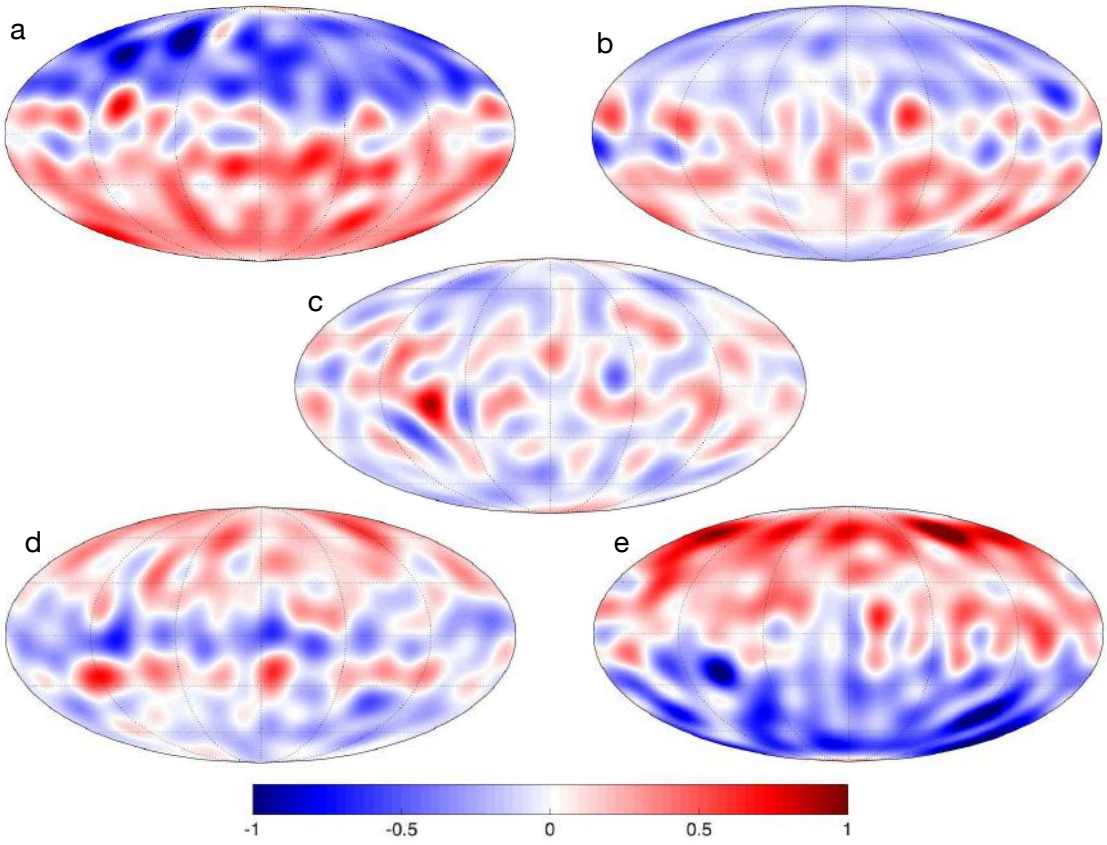

Fig. A1 Radial magnetic field at the outer boundary (CMB) of the model. Magnetic field strength colour bar in units of $\sqrt{\rho\mu_0\eta\Omega} = 8.39 \times 10^{-4}$ T, with $\rho = 1.1 \times 10^4$ kg m^{-3}, $\eta = 0.7$ m^2 s^{-1}, $\Omega = 7.27\times\ 10^{-5}$ s^{-1}. Times of the five snapshots in units of dipole decay time τ_d are a) 59.70, b) 60.12 (first vertical dashed line in Fig. 2), c) 60.48 (second vertical dashed line in Fig. 2, d) 62.20)

To show that our dynamo simulation is Earthlike, we apply diagnostics suggested previously [10]. These diagnostics are included as time series outputs in the dynamo

code (MAGIC) we used, and are computed at the outer boundary (CMB) of the numerical model. Each diagnostic has a nominal value for the geodynamo, and tolerances (see Table 2 in Christensen et al. [10]). The four diagnostic time-series for our simulation, along with nominal values and tolerances, are shown in Fig. A2 and are described as follows. The axial dipolarity, or relative axial dipole power, is the ratio of the axial magnetic dipole field power, which may be represented by $g_{1,0}$ to the sum of the power of all other components of the field up to spherical harmonic degree and order eight. The odd–even ratio, or equatorial symmetry, which is ratio of power of components with odd vs. even values of degree plus order for spherical harmonic degrees between two and eight. The zonality, which is the ratio of zonal (order zero) to non-zonal power power for all components from degree two to eight. The magnetic flux concentration, which is a measure of how strongly the radial magnetic field is concentrated into patches on the CMB surface.

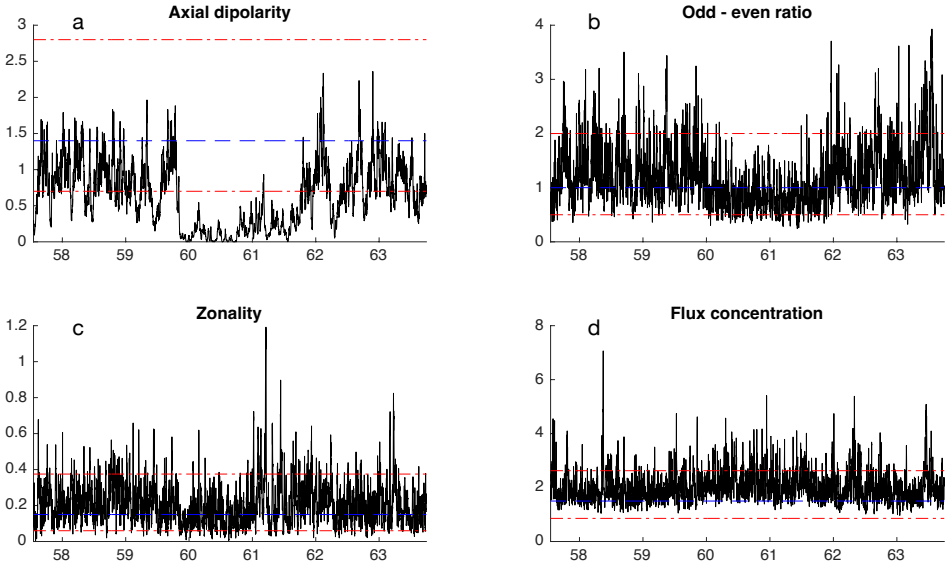

Fig. A2 Diagnostics for Earth-likeness of the magnetic field at the CMB. The diagnostics, including nominal values (dashed blue lines) and tolerances (dot-dashed red lines) are described in [10]. Axial dipolarity (ratio of axial dipole to non-dipolar components), Odd - even ratio (power ratio of odd and even spherical harmonics - equatorial symmetry of the magnetic field) , Zonality (zonal - nonzonal ratio), and (magnetic) flux concentration.

All four diagnostics show that our simulation is Earthlike during times away from the reversal. The diagnostic with the most variation is the axial polarity (Fig. A2a), which typically falls between the nominal value and the lower tolerance during times away from the period of global reversal. During the time period of global reversal ($59.8 \lesssim \tau_d \lesssim 61.8$), the axial polarity falls well below the Earthlike tolerance. The three other diagnostics stay within the Earthlike tolerances away from and throughout the the reversal period. Odd-even ratio decreases from typically above the nominal Earthlike value away from the reversal period to typically below the nominal value during the reversal period. Flux concentration increases slightly during the reversal period. Zonality has no obvious changes comparing the time periods outside and during the polarity reversal.

A.2 Local reversal duration statistics

Local reversal duration statistics from our dynamo simulation are shown in Fig. A3. The cumulative distribution function (CDF) and probability density function (PDF) are displayed for all local reversals, and for SLR and CLR separately. The shortest and longest SLR durations are 109 years and 2.32 kyr. The shortest and longest CLR durations are 1.40 kyr and 13.2 kyr. Thus durations varied 121-fold. Median durations of ~ 2 kyr for all reversals, ~ 1 kyr for SLR, and ~ 5 kyr for CLR can be read from Fig. A3 by noting that the median is half the maximum of the CDF. To ensure non-biased equal area sampling of our numerical simulation, locations are distributed randomly, in an equal-area sense, on the sphere. This step is necessary because the horizontal surface area of r, θ, ϕ grid-cells changes with θ. Thus, sampling on the native grid for the numerical and observational models would introduce a latitudinal bias to the inclination distributions. (See also Heimpel and Evans [44]).

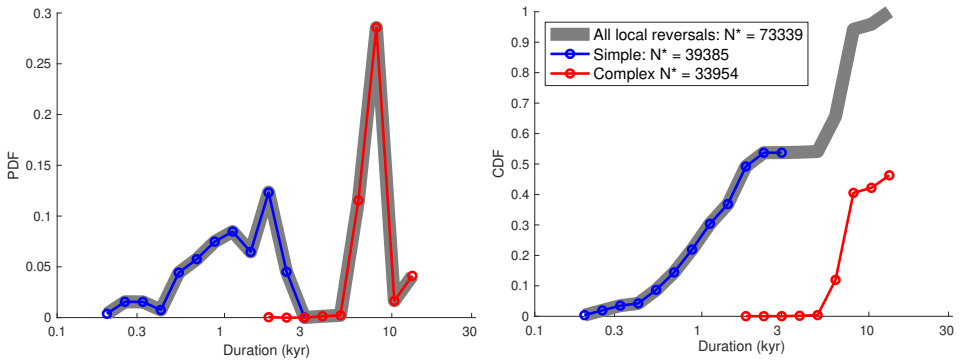

Fig. A3 Reversal duration statistics. Probability density functions (PDF) and Cumulative distribution functions (CDF) for all local reversal durations, and for simple and complex local reversal durations. N* in the equivalent, equal area number of locations.

References

[1] Okada, M., Niitsuma, N.: Detailed paleomagnetic records during the brunhes-matuyama geomagnetic reversal, and a direct determination of depth lag for magnetization in marine sediments. Physics of the Earth and Planetary interiors **56**(1-2), 133–150 (1989)

[2] Sagnotti, L., Scardia, G., Giaccio, B., Liddicoat, J.C., Nomade, S., Renne, P.R., Sprain, C.J.: Extremely rapid directional change during matuyama-brunhes geomagnetic polarity reversal. Geophysical Journal International **199**(2), 1110–1124 (2014)

[3] Macrì, P., Capraro, L., Ferretti, P., Scarponi, D.: A high-resolution record of the matuyama-brunhes transition from the mediterranean region: The valle di manche section (calabria, southern italy). Physics of the Earth and Planetary Interiors **278**, 1–15 (2018)

[4] Clement, B.M.: Dependence of the duration of geomagnetic polarity reversals on site latitude. Nature **428**(6983), 637 (2004)

[5] Valet, J.-P., Meynadier, L., Simon, Q., Thouveny, N.: When and why sediments fail to record the geomagnetic field during polarity reversals. Earth and Planetary

Science Letters **453**, 96–107 (2016)

[6] Valet, J.-P., Fournier, A.: Deciphering records of geomagnetic reversals. Reviews of Geophysics **54**(2), 410–446 (2016)

[7] Haneda, Y., Okada, M., Suganuma, Y., Kitamura, T.: A full sequence of the matuyama–brunhes geomagnetic reversal in the chiba composite section, central japan. Progress in Earth and Planetary Science **7**, 1–22 (2020)

[8] Hoffman, K.A.: Polarity transition records and the geomagnetic dynamo. Science **196**(4296), 1329–1332 (1977)

[9] Clement, B.M., Kent, D.V.: Latitudinal dependency of geomagnetic polarity transition durations. Nature **310**(5977), 488–491 (1984)

[10] Christensen, U.R., Aubert, J., Hulot, G.: Conditions for Earth-like geodynamo models. Earth and Planetary Science Letters **296**(3-4), 487–496 (2010)

[11] Hospers, J.: Remanent magnetism of rocks and the history of the geomagnetic field. Nature **168**(4287), 1111 (1951)

[12] Brynjólfsson, A.: Studies of remanent magnetism and viscous magnetism in the basalts of iceland. Advances in Physics **6**(23), 247–254 (1957)

[13] Einarsson, T.: Magneto-geological mapping in iceland with the use of a compass. Advances in Physics **6**(22), 232–239 (1957)

[14] Opdyke, N.D., Kent, D.V., Lowrie, W.: Details of magnetic polarity transitions recorded in a high deposition rate deep-sea core. Earth and Planetary Science Letters **20**(3), 315–324 (1973) https://doi.org/10.1016/0012-821X(73)90005-8

[15] Channell, J.E., Hodell, D.A., Singer, B.S., Xuan, C.: Reconciling astrochronological and 40ar/39ar ages for the matuyama-brunhes boundary and late matuyama chron. Geochemistry, Geophysics, Geosystems **11**(12) (2010)

[16] Leonhardt, R., Fabian, K.: Paleomagnetic reconstruction of the global geomagnetic field evolution during the matuyama/brunhes transition: iterative bayesian inversion and independent verification. Earth and Planetary Science Letters **253**(1-2), 172–195 (2007)

[17] Spassov, S., Heller, F., Evans, M., Yue, L., Dobeneck, T.v.: A lock-in model for the complex matuyama-brunhes boundary record of the loess/palaeosol sequence at lingtai (central chinese loess plateau). Geophysical Journal International **155**(2), 350–366 (2003)

[18] Sagnotti, L., Giaccio, B., Liddicoat, J.C., Nomade, S., Renne, P.R., Scardia, G., Sprain, C.J.: How fast was the matuyama–brunhes geomagnetic reversal? a new subcentennial record from the sulmona basin, central italy. Geophysical Journal International **204**(2), 798–812 (2016)

[19] Sagnotti, L., Giaccio, B., Liddicoat, J.C., Caricchi, C., Nomade, S., Renne, P.R.: On the reliability of the matuyama–brunhes record in the sulmona basin—comment to 'a reappraisal of the proposed rapid matuyama–brunhes geomagnetic reversal in the sulmona basin, italy'by evans and muxworthy (2018). Geophysical Journal International **216**(1), 296–301 (2019)

[20] Evans, M., Muxworthy, A.: A re-appraisal of the proposed rapid matuyama–brunhes geomagnetic reversal in the sulmona basin, italy. Geophysical Journal International **213**(3), 1744–1750 (2018)

[21] Brown, M.C., Holme, R., Bargery, A.: Exploring the influence of the non-dipole field on magnetic records for field reversals and excursions. Geophysical Journal International **168**(2), 541–550 (2007) https://doi.org/10.1111/j.1365-246X.2006.03234.x http://oup.prod.sis.lan/gji/article-pdf/168/2/541/2012630/168-2-541.pdf

[22] Korte, M., Genevey, A., Constable, C., Frank, U., Schnepp, E.: Continuous geomagnetic field models for the past 7 millennia: 1. a new global data compilation.

Geochemistry, Geophysics, Geosystems **6**(2) (2005)

[23] Glatzmaier, G.A., Roberts, P.H.: A three-dimensional convective dynamo solution with rotating and finitely conducting inner core and mantle. Physics of the Earth and Planetary Interiors **91**(1), 63–75 (1995)

[24] Glatzmaier, G.A., Coe, R.S., Hongre, L., Roberts, P.H.: The role of the earth's mantle in controlling the frequency of geomagnetic reversals. Nature **401**(6756), 885 (1999)

[25] Coe, R.S., Hongre, L., Glatzmaier, G.A.: An examination of simulated geomagnetic reversals from a palaeomagnetic perspective. Philosophical Transactions of the Royal Society of London A: Mathematical, Physical and Engineering Sciences **358**(1768), 1141–1170 (2000)

[26] Olson, P.L., Glatzmaier, G.A., Coe, R.S.: Complex polarity reversals in a geodynamo model. Earth and Planetary Science Letters **304**(1-2), 168–179 (2011)

[27] Wicht, J.: Palaeomagnetic interpretation of dynamo simulations. Geophysical Journal International **162**(2), 371–380 (2005) https://doi.org/10.1111/j.1365-246X.2005.02665.x http://oup.prod.sis.lan/gji/article-pdf/162/2/371/5960946/162-2-371.pdf

[28] Wicht, J., Stellmach, S., Harder, H.: Numerical models of the geodynamo: from fundamental cartesian models to 3d simulations of field reversals. In: Glassmeier, K.-H., Soffel, H., Negendank, J.F.W. (eds.) Geomagnetic Field Variations, pp. 107–158. Springer, Berlin (2009)

[29] Bullard, E.C.: The bakerian lecture, 1967 reversals of the earth's magnetic field. Phil. Trans. R. Soc. Lond. A **263**(1143), 481–524 (1968)

[30] Wicht, J.: Inner-core conductivity in numerical dynamo simulations. Physics of the Earth and Planetary Interiors **132**(4), 281–302 (2002)

[31] Gastine, T., Wicht, J.: Effects of compressibility on driving zonal flow in gas giants. Icarus **219**(1), 428–442 (2012)

[32] Jones, C., Boronski, P., Brun, A., Glatzmaier, G., Gastine, T., Miesch, M., Wicht, J.: Anelastic convection-driven dynamo benchmarks. Icarus **216**(1), 120–135 (2011)

[33] Christensen, U.R.: Geodynamo models: Tools for understanding properties of earth's magnetic field. Physics of the Earth and Planetary Interiors **187**(3-4), 157–169 (2011)

[34] Sprain, C.J., Biggin, A.J., Davies, C.J., Bono, R.K., Meduri, D.G.: An assessment of long duration geodynamo simulations using new paleomagnetic modeling criteria (qpm). Earth and Planetary Science Letters **526**, 115758 (2019)

[35] Kutzner, C., Christensen, U.: From stable dipolar towards reversing numerical dynamos. Physics of the Earth and Planetary Interiors **131**(1), 29–45 (2002)

[36] Jones, C., Schubert, G.: Thermal and compositional convection in the outer core. Treatise in Geophysics, Core Dynamics **8**, 131–185 (2015)

[37] Braginsky, S.I., Roberts, P.H.: Equations governing convection in earth's core and the geodynamo. Geophysical & Astrophysical Fluid Dynamics **79**(1-4), 1–97 (1995)

[38] Fearn, D.R., Loper, D.E.: Compositional convection and stratification of earth's core. Nature **289**(5796), 393 (1981)

[39] Helffrich, G., Kaneshima, S.: Outer-core compositional stratification from observed core wave speed profiles. Nature **468**(7325), 807 (2010)

[40] Kaneshima, S.: Array analyses of smks waves and the stratification of earth's outermost core. Physics of the Earth and Planetary Interiors **276**, 234–246 (2018)

[41] Irving, J.C., Cottaar, S., Lekić, V.: Seismically determined elastic parameters for

earth's outer core. Science advances **4**(6), 2538 (2018)

[42] Gastine, T., Aubert, J., Fournier, A.: Dynamo-based limit to the extent of a stable layer atop earth's core. Geophysical Journal International **222**(2), 1433–1448 (2020)

[43] Olson, P.L., Coe, R.S., Driscoll, P.E., Glatzmaier, G.A., Roberts, P.H.: Geodynamo reversal frequency and heterogeneous core–mantle boundary heat flow. Physics of the Earth and Planetary Interiors **180**(1), 66–79 (2010)

[44] Heimpel, M., Evans, M.: Testing the geomagnetic dipole and reversing dynamo models over earth's cooling history. Physics of the Earth and Planetary Interiors **224**, 124–131 (2013)

[45] Secco, R., Schloessin, H.: The electrical resistivity of solid and liquid fe at pressures up to 7 gpa. Journal of Geophysical Research: Solid Earth (1978–2012) **94**(B5), 5887–5894 (1989)

[46] Bi, Y., Tan, H., Jing, F.: Electrical conductivity of iron under shock compression up to 200 gpa. Journal of Physics: Condensed Matter **14**(44), 10849 (2002)

[47] Koker, N., Steinle-Neumann, G., Vlček, V.: Electrical resistivity and thermal conductivity of liquid fe alloys at high p and t, and heat flux in earth's core. Proceedings of the National Academy of Sciences **109**(11), 4070–4073 (2012)

[48] Pozzo, M., Davies, C., Gubbins, D., Alfè, D.: Thermal and electrical conductivity of iron at earth/'s core conditions. Nature **485**(7398), 355–358 (2012)

[49] Davies, C., Pozzo, M., Gubbins, D., Alfè, D.: Constraints from material properties on the dynamics and evolution of earth's core. Nature Geoscience **8**(9), 678 (2015)